Journal of Assisted Reproduction and Genetics (2023) 40:1447–1459
https://doi.org/10.1007/s10815-023-02815-x

REPRODUCTIVE PHYSIOLOGY AND DISEASE

miR-4433a-3p promotes granulosa cell apoptosis by targeting peroxisome proliferator–activated receptor alpha and inducing immune cell infiltration in polycystic ovarian syndrome

Lin Zhu[1,2] · Xi Yao[1,2] · Ying Mo[1,2] · Ming-wei Chen[1,2] · Si-chen Li[1,2] · Jian-qiao Liu[1,2] · Hai-ying Liu[1,2]

Received: 26 December 2022 / Accepted: 24 April 2023 / Published online: 19 May 2023

Abstract

Background Granulosa cell (GC) proliferation and apoptosis are critical events of the ovum energy supply, which lead to follicular growth retardation or atresia, and various ovulatory obstacles, eventually resulting in the development of ovarian disorders such as polycystic ovarian syndrome (PCOS). Apoptosis and dysregulated miRNA expression in GCs are manifestations of PCOS. miR-4433a-3p has been reported to be involved in apoptosis. However, there is no study reporting the roles of miR-4433a-3p in GC apoptosis and PCOS progression.

Methods miR-4433a-3p and peroxisome proliferator–activated receptor alpha (PPAR-α) levels in GCs of PCOS patients or in tissues of a PCOS rat model were examined by quantitative polymerase chain reaction and immunohistochemistry. Bioinformatics analyses and luciferase assays were used to examine the association between miR-4433a-3p and PPAR-α, as well as PPAR-α and immune cell infiltration, in PCOS patients.

Results miR-4433a-3p expression in GCs of PCOS patients was increased. miR-4433a-3p overexpression inhibited the growth of the human granulosa-like tumor cell line (KGN) and promoted apoptosis, while co-treatment with PPAR-α and miR-4433a-3p mimic rescued miR-4433a-3p-induced apoptosis. PPAR-α was a direct target of miR-4433a-3p and its expression was decreased in PCOS patients. PPAR-α expression was also positively correlated with the infiltration of activated $CD4^+$ T cells, eosinophils, B cells, gamma delta T cells, macrophages, and mast cells, but negatively correlated with the infiltration of activated $CD8^+$ T cells, $CD56^+$ bright natural killer cells, immature dendritic cells, monocytes, plasmacytoid dendritic cells, neutrophils, and type 1 T helper cells in PCOS patients.

Conclusion The miR-4433a-3p/PPAR-α/immune cell infiltration axis may function as a novel cascade to alter GC apoptosis in PCOS.

Keywords miR-4433a-3p · Peroxisome proliferator–activated receptor alpha · Granulosa cell · Polycystic ovary syndrome · Immune cell infiltration

Introduction

Polycystic ovarian syndrome (PCOS) is a metabolic and endocrine disorder in reproductive-age women. Polycystic ovarian syndrome patients often have several seemingly unrelated symptoms such as irregular menstruation, amenorrhea, rare ovulation, or anovulation [1]. In addition to increasing the risks of type 2 diabetes mellitus, insulin resistance, endometrial cancer, and cardiovascular disease, studies have found a non-negligible link between PCOS and low levels of chronic systemic inflammation, with evidence of differentially expressed inflammatory biomarkers in the sera of PCOS patients, including C-reactive protein, and the pro-inflammatory cytokines tumor necrosis factor alpha and interleukin 6

Lin Zhu, Xi Yao, and Ying Mo contributed equally to this work.

✉ Jian-qiao Liu
ljq88gz@163.com

✉ Hai-ying Liu
liuhaiying0606@163.com

[1] Department of Obstetrics and Gynecology, Center for Reproductive Medicine, Guangdong Provincial Key Laboratory of Major Obstetric Diseases, The Third Affiliated Hospital of Guangzhou Medical University, Guangzhou, China

[2] Key Laboratory for Reproductive Medicine of Guangdong Province, The Third Affiliated Hospital of Guangzhou Medical University, Guangzhou, China

[2, 3]. The pathophysiology of PCOS involves a vicious cycle of the combined effects of obesity, insulin resistance, diabetes, and other pro-inflammatory metabolic disorders that eventually lead to chronic low-grade inflammation, hormone disturbances, and low fertility [4]. Polycystic ovarian syndrome is a complex polygenic disorder associated with epigenetic and environmental influences, with aberrant proliferation and apoptosis of granulosa cells (GCs) as the main causes of follicular atresia [5]. Meanwhile, the imbalance between autophagy and apoptosis of GCs determines the outcome of the follicles [6].microRNAs (miRNAs) are highly conserved and short non-coding RNAs of approximately 22 nucleotides which behave as post-transcriptional regulators. microRNAs regulate mRNA expression by binding to complementary 3′-untranslated regions on target mRNAs [7–9]. The aberrant expression or dysfunction of miRNAs can affect multiple cellular processes such as cell proliferation, differentiation, and apoptosis, which in turn modulate follicular development and atresia, as well as hormone synthesis and metabolism, and eventually lead to the development of ovarian disorders such as PCOS [10–12]. microRNAs are also key regulators of diverse physiological processes, such as immune system homeostasis, which protects individuals from excessive inflammation and tissue damage. Aberrant miRNA expression can lead to impaired immune activation and tolerance mechanisms, ultimately resulting in the development of autoimmune disorders and other diseases such as cancer [13, 14].

Peroxisome proliferation–activated receptor (PPAR) is a transcription factor of ligand-activated nuclear receptors family, which includes PPAR-α, PPAR-β/δ, and PPAR-γ, and these transcription factors regulate lipid metabolism, glucose breakdown, energy homeostasis, and inflammation-related gene expression [15]. PPAR-α activation increases fatty acid catabolism, controls inflammation and hepatic triglyceride accumulation, prevents hyperlipidemia, and plays crucial roles in hepatocyte and adipocyte differentiation and lipid metabolism [16, 17]. Moreover, PPAR-γ gene polymorphisms associate with PCOS and regulate progesterone production by GCs [18, 19]. However, the role of PPAR-α in PCOS is unknown.

Here, we examine the roles of miR-4433a-3p and PPAR-α in PCOS and clarify the immune response in PCOS patients. Our study provides new insights on potential therapeutic targets for improving or avoiding adverse outcomes such as poor follicular cell quality, impaired ovulation, and pregnancy loss caused by PCOS.

Materials and methods

Polycystic ovary syndrome gene expression data

Polycystic ovary syndrome dataset (GSE84376) was retrieved from the Gene Expression Omnibus (GEO). The GSE84376 dataset was based on the GPL16384 array (Affymetrix Multispecies miRNA-3 Array), which contained 15 PCOS samples.

The dataset was normalized using "sva" in R. With the microarray platform's data table, the series matrix file was annotated using an approved gene symbol. Files with gene expression matrix were acquired.

Ethics statement

This study was approved by the human ethics committee of the Third Affiliated Hospital of Guangzhou Medical University. Before enrollment, participants signed informed consent forms (ethics review board number: 2018NO:083; Guangzhou, China). Guangzhou Medical University's animal ethics committee approved the animal experiments (protocol number: NX-2019–023, Guangzhou, China). Based on the Guide for the Care and Use of Laboratory Animals published by the National Institutes of Health (Bethesda, MD, USA), this study was conducted. Every attempt was made to minimize the suffering of the animals.

Study subjects

Granulosa cells were collected from 10 PCOS-diagnosed infertile female patients at the Third Affiliated Hospital of Guangzhou Medical University from April 2020 to December 2020. The following Rotterdam 2003 criteria were used to diagnose the enrolled patients with PCOS: (1) anovulation and/or infrequent ovulation; (2) signs of hyperandrogenism or hyperandrogenemia; and (3) ultrasound examination showing more than 12 follicles of 2–9 mm in diameter in both ovaries. We also collected GCs from 10 healthy women of reproductive age (35 years old) without PCOS and with regular menstrual cycles. Women were examined gynecologically during the follicular phase, and histopathological examinations confirmed morphological normality. No participant was previously treated with hormones, including contraceptives, anti-androgens, or insulin sensitizers, which could have influenced the release and metabolism of sex hormone. No participant reported pregnancy at 6 months before enrollment or at registration. Granulosa cells were isolated from patients' follicular fluid as previously described [20, 21].

Clear follicular fluid containing GCs was collected on the day of oocyte retrieval. Red blood cells and lymphocytes were removed by centrifugation with lymph separation solution and red blood cell lysate (BioSharp, Beijing, China), respectively [22]. Granulosa cells were washed in phosphate buffered saline (PBS) and cultured in Dulbecco's modified Eagle medium (DMEM, Gibco, USA) supplemented with 10% fetal bovine serum (FBS, Thermo, USA), 50 mg/mL streptomycin, and 50 U/mL penicillin (Thermo) or resuspended in PBS and stored at − 80℃.

Establishment of PCOS rat model

We obtained 28 female Sprague–Dawley rats aged 25 days (body weight, 80–120 g) from the Chang Sheng Experimental Animal Center (Liaoning, China). First, we established the in vitro PCOS model. For 21 consecutive days, the first group of animals received subcutaneous injections of dehydroepiandrosterone (6 mg/100 g body weight; Sigma-Aldrich, St. Louis, MO, USA) in 0.2 mL of oil, and PCOS was successfully established in all rats. For the second group of animals, 14 rats were subcutaneously injected with 0.2 mL of oil for 21 consecutive days; these rats served as the controls. To confirm that PCOS was successfully established, vaginal cells were collected daily from day 1 to day 23 by irrigation with normal saline, and smears were prepared for observation under an optical microscope. Model establishment was considered successful when there was no complete estrous cycle for several days. Ovaries were collected, fallopian tubes and adipose tissues were removed under an optical microscope, and tissues were rinsed with normal saline to remove red blood cells.

Cell transfection

KGN cells, a GC line, were obtained from the Riken Cell Bank (Wako, Saitama, Japan) [23] and cultured in DMEM supplemented with 5% FBS at 37 °C in a humidified incubator under conditions of 5% CO_2. Cells transfected with miR-4433a-3p mimic (miR10000088-1–5), miR-4433a-3p inhibitor (miR20000088-1–5), or their corresponding negative controls were purchased from RiboBio Biotechnology Co., Ltd. (Guangzhou, China). Control and PPAR-α overexpression (EX-Z5927-M02) vectors were procured from GeneCopoeia (Rockville, MD, USA). Approximately 24 h before transfection, the cells were cultured in polystyrene 6-well plates supplemented with 10% FBS in DMEM. When the cell confluence reached approximately 60%, cell transfection was conducted with the riboFECT CP transfection kit (Guangzhou, China), in accordance with the manufacturer's instructions. An additional processing step was performed approximately 48 h after transfection.

RNA isolation and quantitation

We reverse-transcribed the RNA isolated from GCs of PCOS patients and controls with TRIzol reagent (Thermo Fisher Scientific, Waltham, MA, USA). The SYBR Premix Ex Taq kit (Tli RNaseH Plus) was used for quantitative polymerase chain reactions (q-PCR) on Applied Biosystems' ABI 7500 real-time PCR system (Waltham, MA, USA). A 5-s predenaturation at 94 °C was followed by 30 cycles of denaturation at 94 °C for 30 s, annealing at 54.5 °C for 30 s, and extension at 72 °C for 30 s. Samples were stored at 4 °C for 10 min after extension at 72 °C. miR-4433a-3p expression was quantified with the TaqMan miRNA assay (Ambion, Austin, TX, USA), and the internal control was U6. Primers were prepared by RiboBio Biotechnology Co., Ltd. (Table 1). PPAR-α and miR-4433a-3p expression levels were calculated using the $2-^{\Delta\Delta}$Ct method [24].

Western blot analysis

For the extraction of proteins, sodium dodecyl sulfate–polyacrylamide gel electrophoresis sample loading buffer or the radioimmunoassay lysis buffer was used. BCA kit (Thermo Fisher Scientific) was used to determine protein concentrations, according to the manufacturer's protocol. Subsequently, 40 μg (50 μg/μL) of protein was electrophoresed using 10–12.5% polyacrylamide gels and then transferred it onto polyvinylidene fluoride membranes (Bio-Rad, Hercules, CA, USA). Membranes were blocked for 1 h in 5% skim milk at room temperature, followed by incubation with diluted BCL-2, PPAR-α, cleaved-caspase-3, β-actin, and BAX primary antibodies overnight at 4 °C. After three times of washing with Tris-buffered saline containing Tween 20, membranes were incubated for 1 h with rabbit anti-mouse IgG or goat anti-rabbit IgG conjugated to horseradish peroxidase. All primary and secondary antibodies were purchased from Abcam (Cambridge, MA, USA). Immunoreactive proteins were detected and quantified with the Odyssey CLx Two-color Laser Imaging system (LI-COR, Lincoln, NE, USA) and Image Studio (Alias, San Rafael, CA, USA), respectively.

Acridine orange–ethidium bromide (AO/EB) staining

The apoptosis of KGN cells was detected with the AO/EB kit (BioSharp), and the cells were observed under an XSP-2C microscope (Shanghai Batuo Instrument Co., Ltd.,

Table 1 Primer sequences used for quantitative polymerase chain reaction

Gene	Primer sequence (5′–3′)
miR-4433a-3p	F: TCCTCCTTACGTCCCACC
	R: CCCACCCTGTATTCCTCC
PPAR-α	F: ACGATTCGACTCAAGCTGGT
	R: GTTGTGTGACATCCCGACAG
U6	F: GCTTCGGCAGCACATATACTAAAAT
	R: CGCTTCACGAATTTGCGTGTCAT
GAPDH	F: GTCTCCTCTGACTTCAACAGCG
	R: ACCACCCTGTTGCTGTAGCCAA

Shanghai, China). The apoptosis rate was calculated as follows:

$$\text{Apoptosis rate} = \frac{\text{Apoptotic cells}}{\text{Total cells}} \times 100\%$$

Cell counting kit-8 (CCK-8) assay

The viability of KGN cells was assessed with the CCK-8 kit (Meilunbio Biotechnology Co., Ltd., Dalian, China). Cells (1×10^3) were cultured in polystyrene 96-well plates with DMEM as indicated above, and 20 μL of CCK-8 solution (5 g/L) was added into each well. Plates were incubated for 4 h under dark conditions, and absorbance values at 450 nm on days 0, 1, 2, and 4 were determined with a microplate reader. The cell viability rate was calculated as follows:

$$\text{Cell viability rate} = \frac{\text{As} - \text{Ab}}{\text{Ac} - \text{Ab}} \times 100\%$$

where As is the absorbance in the experimental group, Ab is the absorbance in the control group, and Ac is the absorbance in the blank.

Flow cytometry

KGN cells (1×10^6–1×10^7 cells) were cultured in polystyrene 6-well plates for 48 h as indicated above. In conjunction with the FACScan flow cytometer (Becton Dickinson, San Jose, CA, USA) and CellQuest software (Becton Dickinson), the Annexin V-fluorescein isothiocyanate (FITC)/propidium iodide (PI) apoptosis kit was used to assess apoptosis.

Luciferase reporter gene assay with dual luciferases

A dual-luciferase reporter gene assay was utilized to identify the sites of binding between miR-4433a and PPAR-α. The *Ppar-alpha* sequence was amplified and purified. In the next step, wild-type PPAR-α (PPAR-α-Wt, containing the miR-4433a-3p binding site) and mutant PPAR-α (PPAR-α-Mut, with the miR-4433a-3p binding site mutated) fragments were inserted into the pMIRreporter vector (RiboBio Biotechnology Co., Ltd.) by endonuclease cleavage (SpeI and HindIII) and ligated overnight at 4 °C with T4 DNA ligase. Next, DNA extracted from transfected KGN cells was cleaved with restriction endonucleases and sequenced to identify the plasmids. The putative luciferase reporter plasmids PPAR-α-WT and PPAR-α-Mut were co-transfected with miR-4433a-3p mimic into KGN cells. Luciferase activity was measured approximately 48 h after transfection with a luciferase detection kit (Beyotime Biotechnology Co., Ltd., Shanghai, China).

Hematoxylin – eosin staining and immunohistochemistry

Fixed ovarian tissues were sectioned and mounted onto polylysine-coated glass slides and dried overnight at 60 °C, followed by staining with hematoxylin–eosin. Based on previously described methods [25], immunohistochemistry (IHC) and immunofluorescence were used to evaluate protein concentration and localization. A graded series of ethanol solutions were used to dewax the sections. The sections were blocked with 3% bovine serum albumin (BSA) at 37 °C and poured away. Then, we incubated sections overnight with an antibody against PPAR-α (1: 200, ab245119, Abcam, Cambridge, UK) at 4 °C. Sections were incubated with a secondary antibody (1:2000) for 2 h at 25 °C. Optical microscopy was used to observe the sections after avidin-biotinylated-peroxidase complex staining and DAB staining techniques were applied. For immunofluorescence, 4,6-diamidino-2-phenylindole (DAPI) (1:2000, Beyotime) was used to stain nuclei, and sections were observed under an Olympus laser scanning confocal microscope (Tokyo, Japan). Researchers with more than 5 years of routine histological experience calculated the number and proportion of corpus luteum and follicles at different developmental stages.

Functional enrichment analysis of PPAR-α co-expressed genes

To explore the biological roles of PPAR-α co-expressed genes in PCOS, all co-expressed genes were uploaded into Metascape (http://metascape.org) for GO analysis. In order to analyze pathways, MSigDB of Hallmark Gene Sets and KEGG of Kyoto Encyclopedia of Genes and Genomes were used. Based on their Kappa scores > 0.3, p-values < 0.05, enrichment factor values > 1.5, and a minimum count of 3, genes were obtained and clustered. The most statistically significant term in a set was selected as the cluster. In cases where > 20 terms were identified for a pathway or GO annotation, the top 20 terms were selected for visualization.

Gene Set Enrichment Analysis (GSEA) of the genes co-expressed with PPAR-α

To understand the biological significance of PPAR-α co-expressed genes, we performed Gene Ontology (GO) enrichment analysis using GSEA. GSEA is a valuable approach for evaluating genome-wide expression profile

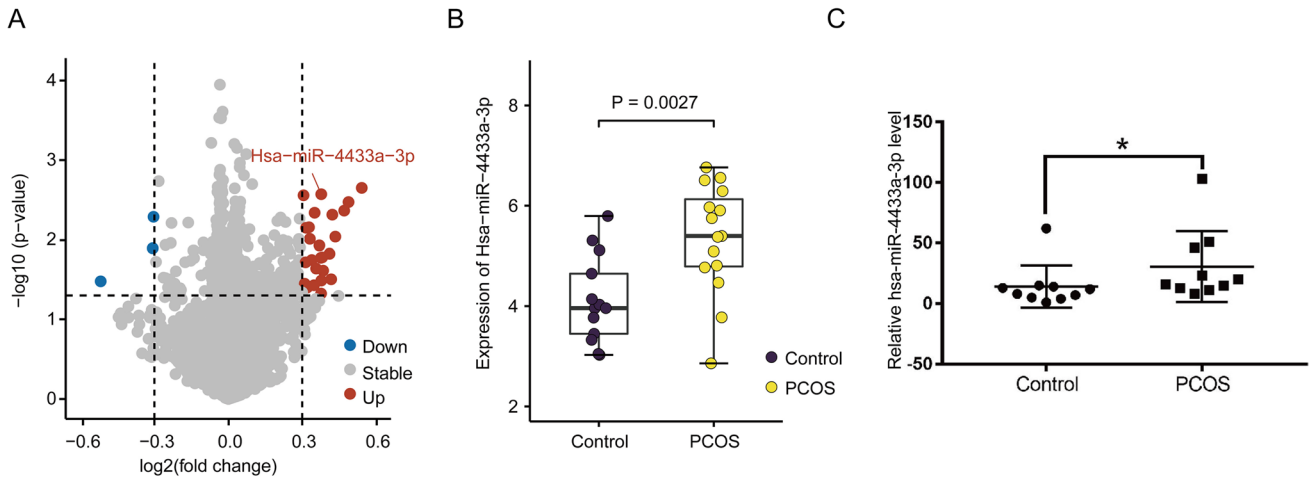

Fig. 1 miR-4433a-3p expression is up-regulated in PCOS patients. **A** Expression of differentially expressed miRNAs in PCOS patients in the GEO dataset. **B** Expression of miR-4433a-3p in PCOS patients in the GEO dataset. **C** Expression of miR-4433a-3p in GCs of PCOS patients by q-PCR. Data are presented as mean ± standard deviation, $n = 3$–6 for each group. $^{*}p < 0.05$ vs. control group

data, as it identifies different aspects of cell function by contrasting genes with predefined gene sets. A group of genes sharing pathways, localization features, functions, and other characteristics is referred to as a gene set. GSEA was performed using the cluster profile package. The Pearson correlation coefficient of each gene co-expressed with PPAR-α was calculated to generate a list of genes according to changes in this parameter.

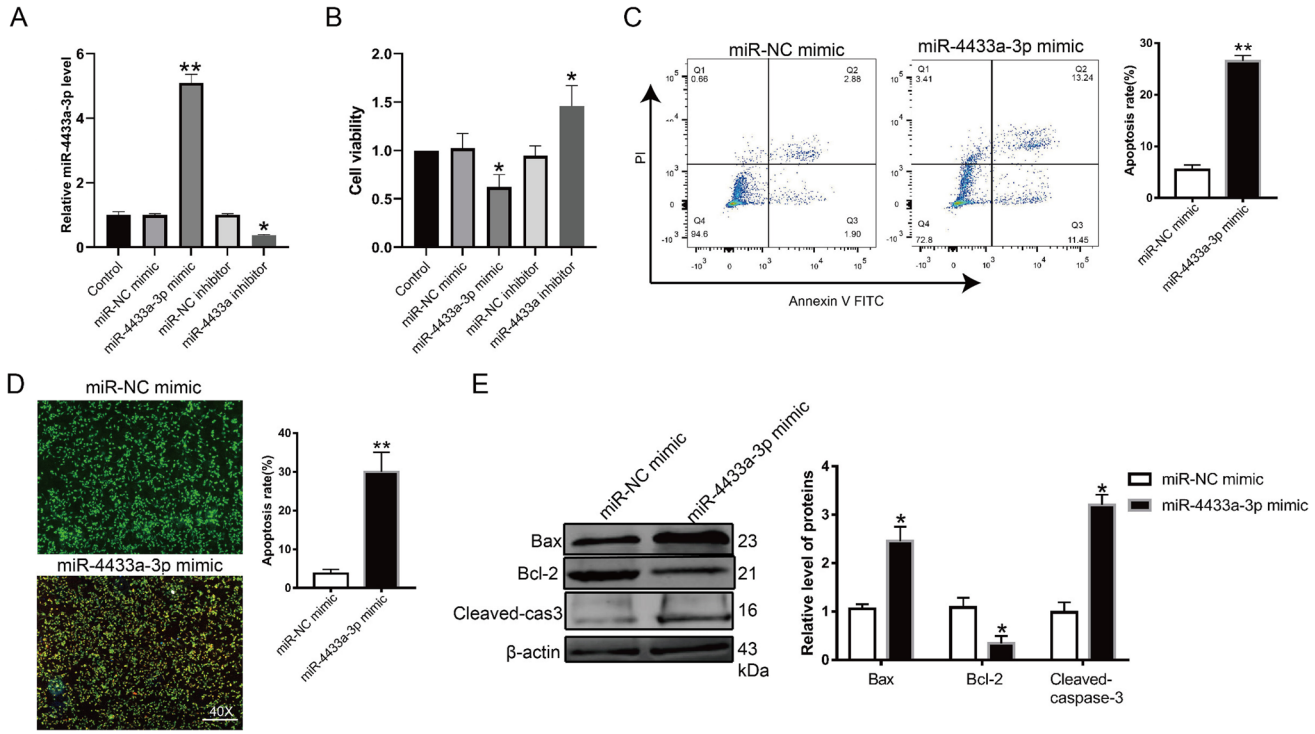

Fig. 2 miR-4433a-3p regulates growth and apoptosis of KGN cells. **A** Expression of miR-4433a-3p in KGN cells after transfection with miR-4433a-3p mimic or inhibitor. **B** Results of the CCK-8 assay examining KGN cell viability after transfection with miR-4433a mimic or inhibitor. **C**, **D** Results of flow cytometry and the AO/EB assay showing apoptosis of KGN cells. **E** BAX, BCL-2, and cleaved-caspase-3 protein levels after transfection with miR-4433a-3p mimic or control. $n = 3$–6 for each group. $^{*}p < 0.05$ vs. the miR-NC group, $^{**}p < 0.01$ vs. miR-NC group, $^{ns}p > 0.05$ vs. control group

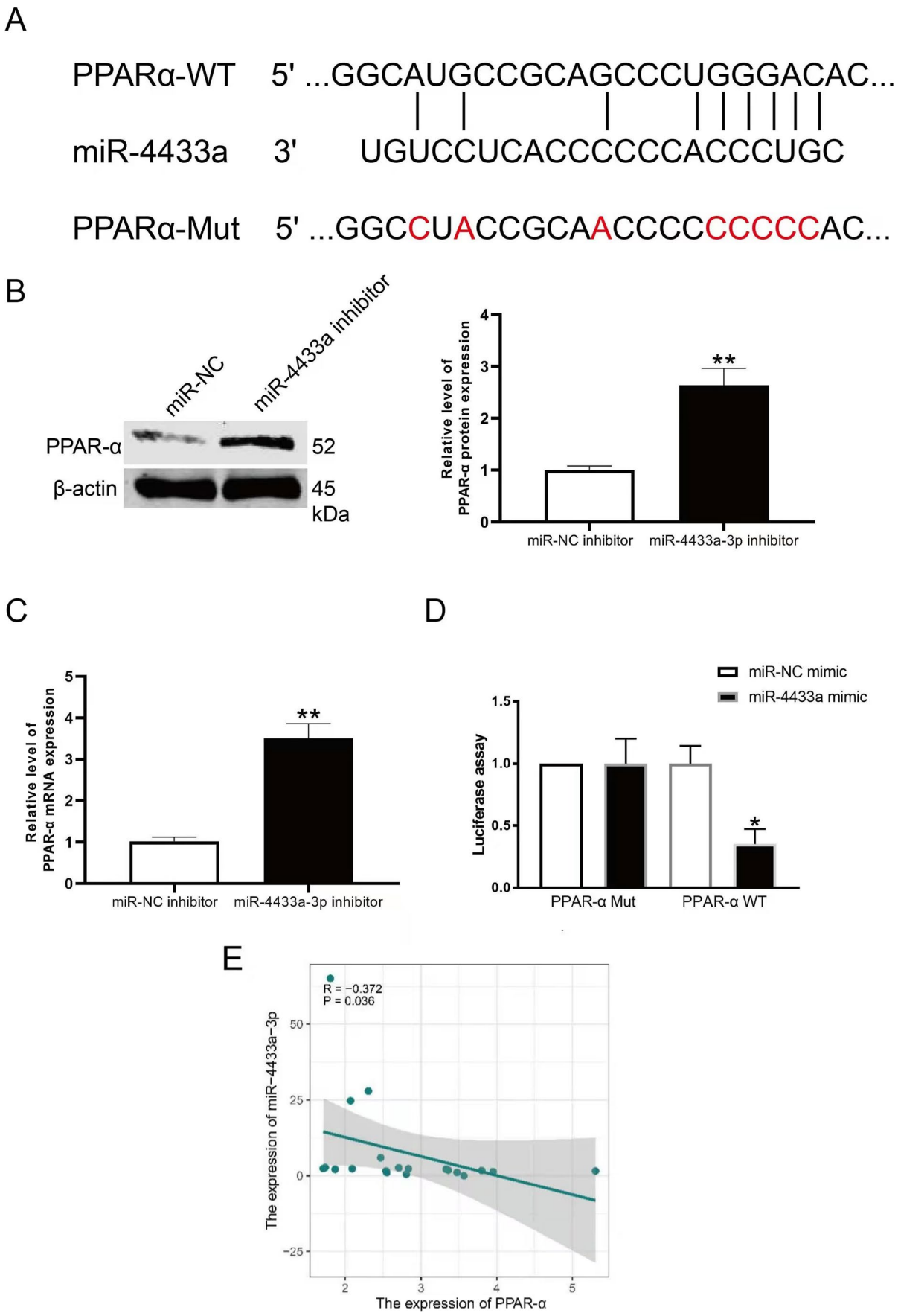
A
PPARα-WT 5' ...GGCAUGCCGCAGCCCUGGGACAC...
miR-4433a 3' UGUCCUCACCCCCCACCCUGC
PPARα-Mut 5' ...GGCCUACCGCAACCCCCCCCCAC...
B
miR-NC
miR-4433a inhibitor
PPAR-α
β-actin
52
45
kDa
Relative level of PPAR-α protein expression
miR-NC inhibitor
miR-4433a-3p inhibitor
C
Relative level of PPAR-α mRNA expression
miR-NC inhibitor
miR-4433a-3p inhibitor
D
miR-NC mimic
miR-4433a mimic
Luciferase assay
PPAR-α Mut
PPAR-α WT
E
R = −0.372
P = 0.036
The expression of miR−4433a−3p
The expression of PPAR-α

◂**Fig. 3** PPAR-α is directly targeted by miR-4433a-3p. **A** Seed units between miR-4433a-3p and PPAR-α. **B**, **C** Protein and mRNA levels of PPAR-α in GCs after transfection with miR-4433a-3p inhibitor or control by western blot and q-PCR. **D** Results of luciferase reporter assays showing the relationship between miR-4433a-3p and PPAR-α. **E** Correction of miR-4433a-3p and PPAR-α in GCs of PCOS patients. $n = 3$–6 for each group. $*p < 0.05$ vs. control or miR-NC group, $**p < 0.01$ vs. control or the miR-NC group

Immune infiltration analysis

Using Single-Sample Gene Set Enrichment Analysis software (ssGSEA), we calculated enrichment scores for 782 genes representing 28 different immune cell types in R (GSVA package).

Statistical analysis

In this study, the mean and standard deviation of measurement data with normal distributions were computed using SPSS 21.0 software (IBM Corp., Armonk, NY, USA). Interquartile ranges were used for data with skewed distributions and abnormal variances. To compare groups, a *t*-test was applied to independent samples. Skewed data was calculated in R (GSVA package) using the Wilcoxon signed-rank test. One-way ANOVA with Tukey's post hoc test was used for multiple group comparisons. Data collection at different times was analyzed using repeated-measures ANOVA with Tukey's post hoc test. To analyze correlations, the Pearson correlation coefficient was used. Chi-square tests were used to compare enumeration data, which were expressed as percentages. Statistical significance was determined by *p*-values of less than 0.05.

Results

miR-4433a-3p expression is up-regulated in patients with PCOS

GEO datasets (GSE84376) were retrieved from the GEO to examine the expression of specific miRNAs in GCs isolated from the follicular fluid of 15 PCOS patients and 13 healthy participants. Student's *t*-test and fold-change comparisons were applied to evaluate the expression of miRNAs between the two groups of samples (the threshold was set to $p < 0.05$, $|\log2FD| > 1$). A total of 13 miRNAs were selected for further analyses, of which 12 were up-regulated and 1 was down-regulated (Fig. 1A). The *p*-value of miR-4433a-3p, whose level was increased in PCOS patients compared to healthy participants, was 0.0027 (Fig. 1B). We isolated GCs from 10 PCOS patients and 10 healthy participants to validate the microarray results by q-PCR. Compared to healthy participants, miR-4433a-3p expression was up-regulated in PCOS patients (Fig. 1C)

miR-4433a-3p overexpression inhibits growth and induces apoptosis of KGN cells

The aberrant expression of miR-4433a-3p in GCs of PCOS patients implicates it as a potential mediator of apoptosis. To test this hypothesis, KGN cells were stably transfected with miR-4433a-3p mimic, miR-4433a-3p inhibitor, or the corresponding controls. Compared to controls, miR-4433a-3p expression was increased after transfection with the mimic, whereas it was decreased after transfection with the inhibitor ($p < 0.05$; Fig. 2A). The results of the CCK-8 assay revealed that miR-4433a-3p inhibitor increased cell viability, whereas miR-4433a-3p mimic decreased cell viability ($p < 0.05$; Fig. 2B). Furthermore, the results of flow cytometry demonstrated increased apoptosis after transfection with the mimic (Fig. 2C), consistent with the results of the dual acridine orange/ethidium bromide (AO/EB) fluorescent staining assay (Fig. 2D). Thus, increased miR-4433a-3p expression reduces cell viability and induces apoptosis. The results of western blot analysis revealed that transfection with miR-4433a-3p mimic decreased the level of BCL-2 (an anti-apoptotic protein) and increased the levels of cleaved-caspase3 and BAX (pro-apoptotic proteins) in KGN cells ($p < 0.05$; Fig. 2E).

PPAR-α is a direct target of miR-4433a in granulosa cells

Bioinformatics analyses showed that the PPAR-α signaling pathway plays an important role in the regulation of miR-4433a-3p expression in PCOS patients (Fig. S1). We used bioinformatics analyses to predict the specific sites of binding between PPAR-α and miR-4433a-3p, and our data indicated that PPAR-α is a direct target of miR-4433a-3p (Fig. 3A). The results of q-PCR and western blot analyses revealed the increased PPAR-α expression in KGN cells after transfection of miR-4433a inhibitor, and PPAR-α expression was negatively correlated with miR-4433a-3p expression in KGN cells (Fig. 3B, C). Next, we evaluated PPAR-α expression after overexpression of PPAR-α (Fig. S2). PPAR-α overexpression significantly increased the PPAR-α protein level in KGN cells, indicative of successful in vitro transfection. No difference in the relative luciferase activity of KGN cells after co-transfection of PPAR-α-Mut and miR-4433a-3p mimic was observed ($p > 0.05$). However, the relative luciferase activity was decreased after co-transfection of PPAR-α-WT and miR-4433a-3p mimic ($p < 0.05$; Fig. 3D). Furthermore, there was a negative correlation between miR-4433a-3p and PPAR-α in GCs of PCOS patients ($R = -0.372$, $p = 0.036$) by the Pearson correlation coefficient (Fig. 3E), indicating that miR-4433a-3p directly targets PPAR-α expression in PCOS.

PPAR-α overexpression inhibits the effects of miR-4433a-3p on the apoptosis of KGN cells

To further confirm the role of PPAR-α in KGN cell apoptosis, we examined the PPAR-α protein level after transfection of miR-4433a-3p mimic or miR-4433a-3p mimic + PPAR-α overexpression plasmid (Fig. 4A) and observed increased PPAR-α expression. We also examined PPAR-α expression after transfection of miR-4433a-3p mimic (Fig. 4B). CCK-8 assays were used to evaluate the viability of KGN cells after transfection of miR-4433a-3p mimic + PPAR-α overexpression plasmid. No difference in the cell viability of the miR-4433a-3p mimic + PPAR-α overexpression plasmid group was observed compared to the control group. However, the cell viability of the miR-4433a-3p mimic group was decreased compared to the control group (Fig. 4C). Compared to cells transfected with miR-4433a-3p mimic + empty vector, apoptosis was significantly decreased in cells transfected with miR-4433a-3p mimic + PPAR-α overexpression plasmid (Fig. 4D).

PPAR-α expression is decreased in PCOS patients

To examine the expression of PPAR-α in PCOS, we isolated GCs from 10 patients with PCOS (PCOS group) and 10 healthy participants (Control group) and found that PPAR-α expression was decreased in GCs of PCOS patients compared to healthy participants (Fig. 5A). By immunohistochemistry, we examined PPAR-α expression in ovarian tissues of a PCOS rat model and found that PPAR-α expression was decreased in ovarian tissues (Fig. 5B).

GSEA-based GO analysis reveals the downstream pathways

The top 5 significantly enriched GO terms in the GSEA dataset were based on GO biological processes. Genes were highly correlated with "immune response-activating signal transduction (GO:0002757)," "activation of immune response (GO:0002253)," "innate immune response (GO:0045087)," "mast cell activation involved in immune

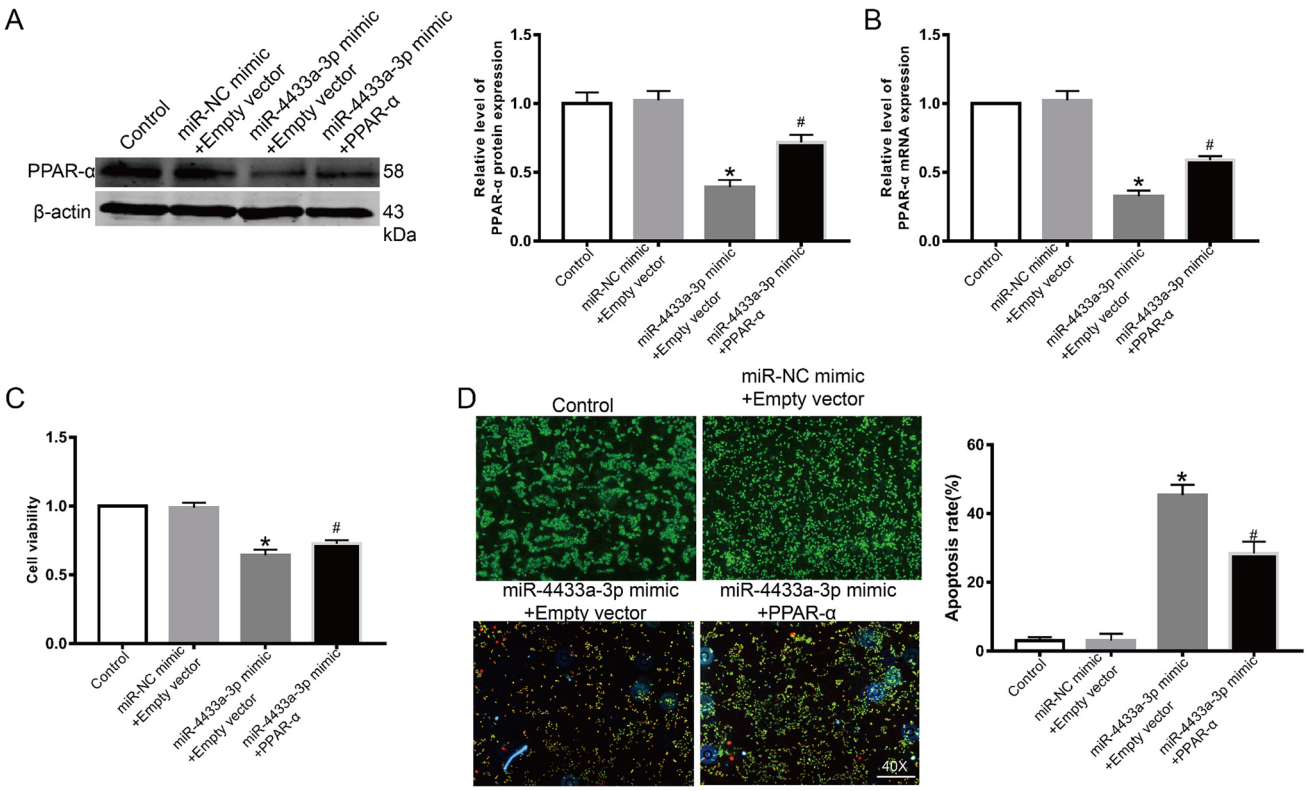

Fig. 4 PPAR-α reverses the effect of miR-4433a-3p mimic on the growth of KGN cells. **A**, **B** Protein and mRNA levels of PPAR-α in KGN cells after transfection of miR-4433a-3p mimic or miR-4433a-3p mimic + PPAR-α overexpression plasmid. **C** Viability of KGN cells after transfection of miR-4433a-3p mimic or miR-4433a-3p mimic + PPAR-α overexpression plasmid. **D** Apoptotic rate of KGN cells as assessed by the AO/EB assay. $n = 3–6$ for each group. $^{*}p < 0.05$ vs. miR-NC mimic + empty vector group, $^{\#}p < 0.05$ vs. miR-4433a-3p mimic + empty vector group, $^{ns}p > 0.05$ vs. control group

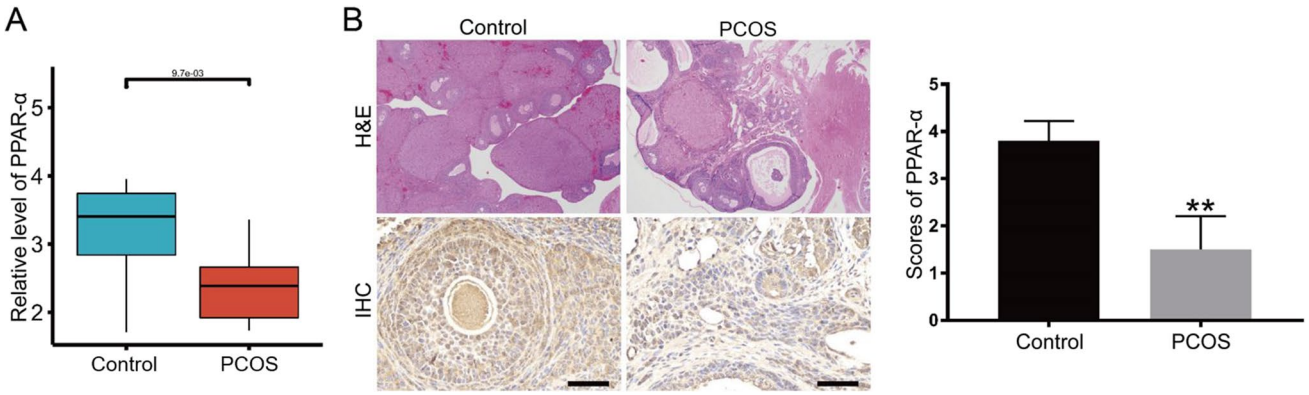

Fig. 5 *PPAR-α* expression is decreased in PCOS patients and a PCOS rat model. **A** Expression of PPAR-α in GCs of PCOS patients by q-PCR. **B** Results of immunohistochemistry showing PPAR-α expression in ovarian tissues of a PCOS rat model. Data are presented as mean ± standard deviation, $n = 3$–6 for each group. $^{**}p < 0.01$ vs. control group

response (GO:0002279)," and "neutrophil activation in immune response (GO:0002283)."

Relationship between PPAR-α and immune cell infiltration in PCOS

In the expression profiles of PCOS, 299 genes with an absolute value of |Pearson correlation coefficient|> 0.95 were selected as PPAR-α co-expressed genes. To evaluate the biological functions of the co-expressed genes, we performed ssGSEA and found that PPAR-α expression associated with immune response–activating signal transduction, immune response activation, innate immune response activation, mast cell activation during the immune response, and neutrophil activation of the immune response signaling pathway (Fig. 6A). Next, we applied ssGSEA to examine the association between PPAR-α expression and immune cell infiltration (Fig. 6B). The ssGSEA data showed that PPAR-α expression was significantly positively correlated with the infiltration of activated B cells ($R = 0.7$, $p = 0.0025$), activated $CD4^+$ T cells ($R = 0.87$, $p < 0.0001$), central memory $CD4^+$ T cells ($R = 0.76$, $p = 0.0007$), effector memory $CD4^+$ T cells ($R = 0.84$, $p < 0.0001$), eosinophils ($R = 0.86$, $p < 0.0001$), gamma delta T cells ($R = 0.89$, $p < 0.0001$), immature B cells ($R = 0.81$, $p = 0.00014$), macrophages ($R = 0.85$, $p < 0.0001$), mast cells ($R = 0.82$, $p = 0.00011$), type 2 T helper cells ($R = 0.86$, $p < 0.0001$), and type 17 T helper cells ($R = 0.92$, $p < 0.0001$), and significantly negatively correlated with activated $CD8^+$ T cells ($R = -0.83$, $p < 0.0001$), $CD56^+$ bright natural killer cells ($R = -0.87$, $p < 0.0001$), immature dendritic cells ($R = -0.8$, $p = 0.0002$), monocytes ($R = -0.85$, $p < 0.0001$), neutrophils ($R = -0.53$, $p = 0.035$), plasmacytoid dendritic cells ($R = -0.92$, $p < 0.0001$), and type 1 T helper cells ($R = -0.89$, $p < 0.0001$) (Fig. 6C).

Discussion

The dysregulation of miRNAs has been implicated in several metabolic disorders such as PCOS. The pathogenesis of PCOS involves GC apoptosis. Thus, we explored the effects of miR-4433a-3p on GC apoptosis, while monitoring its impact on the molecules and mechanisms involved in PCOS. We observed that miR-4433a-3p is a direct target of PPAR-α and immune cell infiltration is associated with KGN cell apoptosis in PCOS.

In this study, we validated the microarray results using GCs of patients with and without PCOS and verified the molecules and mechanisms related to the proliferation and apoptosis of KGN cells. KGN cells may not fully reflect the biology of GCs in humans. Theoretically, non-luteinized GCs are the most ideal cell model for PCOS research. However, due to limitations in existing technologies, most investigators fail to obtain enough non-luteinized GCs from humans. Moreover, compared with primary GCs, it is easier to achieve cell stability and transfection efficiency when using the KGN cell line, which is supported by numerous studies that have used the KGN cell line for PCOS research [26, 27].

Our initial study used the GEO dataset to examine miR-4433a-3p expression in GCs isolated from PCOS patients and control participants during oocyte collection for in vitro fertilization (IVF). Aberrant miR-4433a-3p expression was first reported in papillary thyroid cancer [28]. Wu et al. reported that elevated miR-4433 expression can induce chronic myelogenous leukemia cell apoptosis by targeting the BCR–ABL axis [29]. Interestingly, our results revealed that miR-4433a-3p expression was up-regulated in GCs of PCOS patients and rat ovarian tissues. At the same time, miR-4433a-3p mimic could inhibit KGN cell growth and

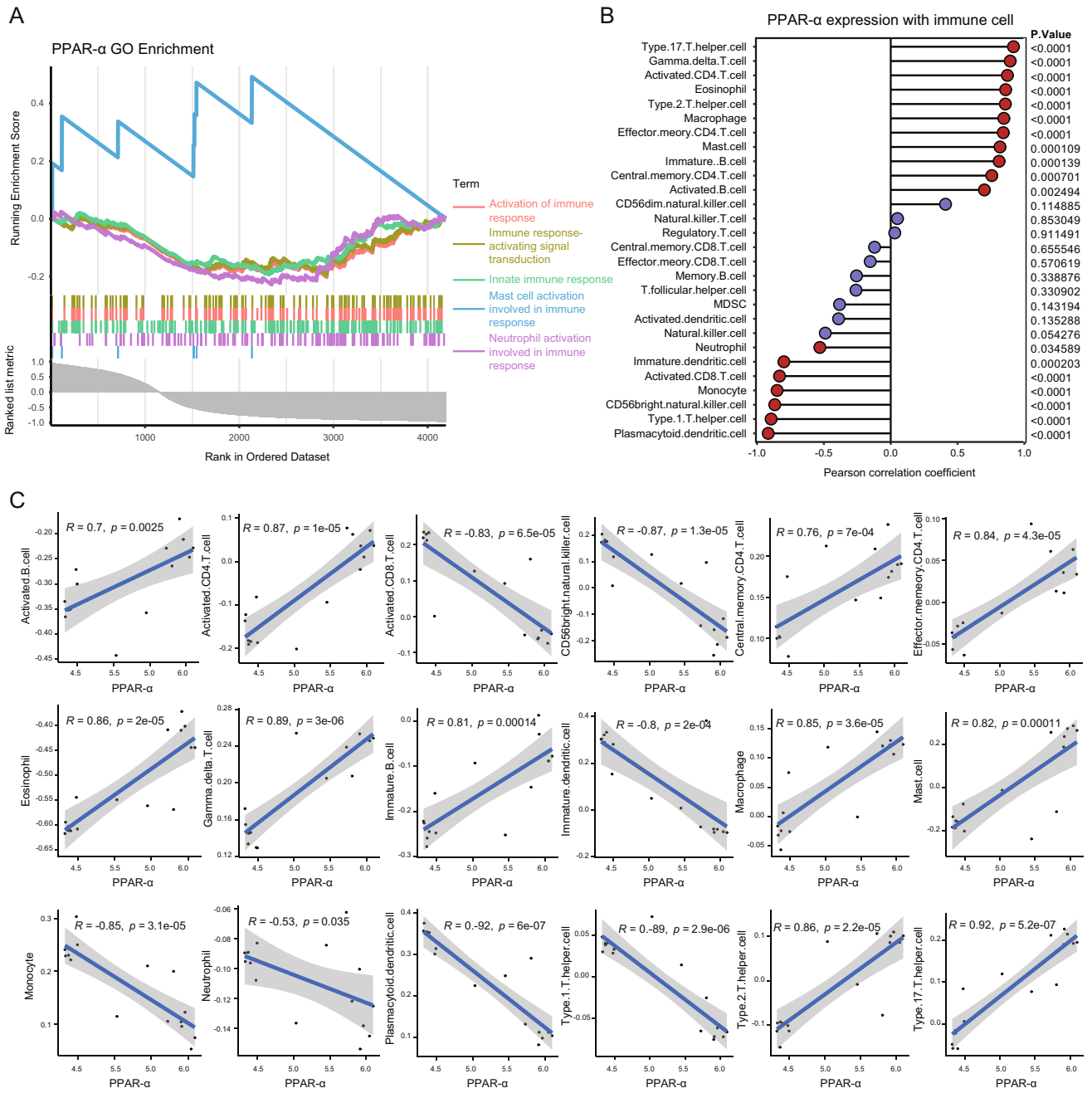

Fig. 6 Functional analysis of PPAR-α and correlation with immune cell infiltration in PCOS. (**A**) ssGSEA pathway enrichment analysis of PPAR-α-associated genes. (**B**) PPAR-α expression in immune cells. (**C**) Correlation of PPAR-α expression with immune cell infiltration in PCOS

induce apoptosis by decreasing Bcl-2 expression and increasing Bax and cleaved-caspase 3 expression, indicating that BCL-2, BAX, and cleaved-caspase 3 play important roles in apoptosis during PCOS progression [30, 31]. On the other hand, the miR-4433a inhibitor could significantly promote KGN cell proliferation and growth, revealing that miR-4433a-3p plays a significant role in PCOS.

In this study, bioinformatics analysis predicted that PPAR-α was a direct target of miR-4433a-3p, consistent with the data of dual-luciferase reporter gene assays. miR-4433a-3p expression was negatively correlated with that of PPAR-α in GCs of PCOS patients. PPAR-α expression is implicated in male and female infertility, where it contributes to gonadal malformations, impaired spermatogenesis, and premature ovarian failure [32–34]. In addition, PPAR-α plays roles in lipid deposition [35], glucose metabolism, overall energy homeostasis, and inflammation-related gene expression [36]. Our results showed that PPAR-α expression

was decreased in GCs of PCOS patients and ovarian tissues of the PCOS rat model.

Peroxisome proliferator–activated receptor (PPAR) is implicated in cell differentiation, steroidogenesis, and gonadal tissue remodeling [33]. In rats, activation of both PPAR-γ and PPAR-α by mono-(2-ethylhexyl) phthalate, an environmental toxicant, affects GC differentiation and metabolism [37]. The functions of PPARs are also closely linked in reproductive tissues from gametogenesis to parturition [38]. Based on these findings, we conclude that PPAR-α influences GC function and follicle development in PCOS patients.

The immune system is important in female reproductive function, with macrophages playing critical roles in uterine function [39, 40]. Macrophages are present throughout the endometrium [41]; they are also present within the lumens of superficial glands [42]. They are enriched at times of inflammation, such as endometrial cancer, endometrial hyperplasia, implantation, and the secretory phase (particularly prior to menses) [43], and uterine macrophages secrete cytokines, growth factors, and chemokines during normal and abnormal events. For example, metformin regulates cyclooxygenase-2 and nitric oxide synthase expression in uterine tissues, as well as serum tumor necrosis factor alpha levels, during recovery from dehydroepiandrosterone-induced hyperandrogenism [44, 45]. These findings suggest that PPAR-α has an anti-inflammatory role by promoting the infiltration of macrophages in patients with PCOS. T cells are also critical for the normal function of the female reproductive system [46, 47]. The proportions of $CD4^+$ T (helper/inducer) and $CD8^+$ T (cytotoxic/suppressor) cells are up-regulated in retroperitoneal [48] or lumbar lymph nodes [49, 50], ovarian tissues [51], and uterine tissues [52]. In this study, PPAR-α expression promoted the infiltration of activated $CD4^+$ T, as well as central memory $CD4^+$ T cells and effector memory $CD4^+$ T cells in PCOS patients, [52, 53]. We also showed that PPAR-α could decrease the proportions of $CD56^+$ bright natural killer cells and immature dendritic cells. Furthermore, macrophages, $CD4^+$ T cells, and $CD8^+$ T cells can release pro-inflammatory mediators to regulate the function of the uterus. Here, we reported that PPAR-α significantly decreased immune cell infiltration in the PCOS model. Targeting these inflammatory processes by different pro-inflammatory mediators can be an alternative approach to the currently available treatments for PCOS that are caused by hyperandrogenism.

In conclusion, miR-4433a-3p and PPAR-α are potential biomarkers in PCOS patients. PPAR-α regulates several immune parameters of ovarian function and hyperandrogenism. This study provides new insights on the clinical implications of miR-4433a-3p and PPAR-α in the treatment of PCOS.

Supplementary Information The online version contains supplementary material available at https://doi.org/10.1007/s10815-023-02815-x.

Author contribution LZ and XY analyzed and interpreted the patient data regarding the PCOS. YM, MWC, and SCL performed the histological examination of the ovarian and animal experiment. HYL and JQL were major contributors in writing the manuscript. All authors read and approved the final manuscript.

Funding This research was supported by the National Natural Science Foundation of China (No. 81801532).

Data availability The datasets used and/or analyzed during the current study are available from the corresponding author on reasonable request, and in the Gene Expression Omnibus (GEO) repository. GSE84376 (https://www.ncbi.nlm.nih.gov/geo/query/acc.cgi?acc=GSE84376).

Declarations

Ethics approval and consent to participate All study protocols were approved by the Institutional Ethics Committee of the Third Affiliated Hospital Guangzhou Medical University (Ethics Review Board, 2018NO:083; Guangzhou, China).

Consent for publication Not applicable.

Competing interests The authors declare no competing interests.

References

1. Nandi A, Chen Z, Patel R, Poretsky L. Polycystic ovary syndrome. Endocrinol Metab Clin North Am. 2014;43(1):123–47.
2. Li Y, Zheng Q, Sun D, et al. Dehydroepiandrosterone stimulates inflammation and impairs ovarian functions of polycystic ovary syndrome. J Cell Physiol. 2019;234(5):7435–47.
3. Rostamtabar M, Esmaeilzadeh S, Tourani M, et al. Pathophysiological roles of chronic low-grade inflammation mediators in polycystic ovary syndrome. J Cell Physiol. 2021;236(2):824–38.
4. Jeanes YM, Reeves S. Metabolic consequences of obesity and insulin resistance in polycystic ovary syndrome: diagnostic and methodological challenges. Nutr Res Rev. 2017;30(1):97–105.
5. Zheng Q, Li Y, Zhang D, et al. ANP promotes proliferation and inhibits apoptosis of ovarian granulosa cells by NPRA/PGRMC1/EGFR complex and improves ovary functions of PCOS rats. Cell Death Dis. 2017;8(10):e3145.
6. Lin M, Hua R, Ma J, et al. Bisphenol A promotes autophagy in ovarian granulosa cells by inducing AMPK/mTOR/ULK1 signalling pathway. Environ Int. 2021;147:106298.
7. Imbar T, Eisenberg I. Regulatory role of microRNAs in ovarian function. Fertil Steril. 2014;101(6):1524–30.
8. Stahlhut C, Slack FJ. MicroRNAs and the cancer phenotype: profiling, signatures and clinical implications. Genome Med. 2013;5(12):111.
9. Fu X, He Y, Wang X, et al. MicroRNA-16 promotes ovarian granulosa cell proliferation and suppresses apoptosis through targeting PDCD4 in polycystic ovarian syndrome. Cell Physiol Biochem. 2018;48(2):670–82.
10. Robinson CL, Zhang L, Schutz LF, Totty ML, Spicer LJ. MicroRNA 221 expression in theca and granulosa cells: hormonal regulation and function. J Anim Sci. 2018;96(2):641–52.

11. Kong F, Du C, Wang Y. MicroRNA-9 affects isolated ovarian granulosa cells proliferation and apoptosis via targeting vitamin D receptor. Mol Cell Endocrinol. 2019;486:18–24.
12. Tesfaye D, Gebremedhn S, Salilew-Wondim D, et al. MicroRNAs: tiny molecules with a significant role in mammalian follicular and oocyte development. Reproduction. 2018;155(3):R121–35.
13. Peng L, Chen Z, Chen Y, Wang X, Tang N. MIR155HG is a prognostic biomarker and associated with immune infiltration and immune checkpoint molecules expression in multiple cancers. Cancer Med. 2019;8(17):7161–73.
14. Yuan X, Berg N, Lee JW, et al. MicroRNA miR-223 as regulator of innate immunity. J Leukoc Biol. 2018;104(3):515–24.
15. Bougarne N, Weyers B, Desmet SJ, et al. Molecular actions of PPARalpha in lipid metabolism and inflammation. Endocr Rev. 2018;39(5):760–802.
16. Pawlak M, Lefebvre P, Staels B. Molecular mechanism of PPARalpha action and its impact on lipid metabolism, inflammation and fibrosis in non-alcoholic fatty liver disease. J Hepatol. 2015;62(3):720–33.
17. Preidis GA, Kim KH, Moore DD. Nutrient-sensing nuclear receptors PPARalpha and FXR control liver energy balance. J Clin Invest. 2017;127(4):1193–201.
18. San-Millan JL, Escobar-Morreale HF. The role of genetic variation in peroxisome proliferator-activated receptors in the polycystic ovary syndrome (PCOS): an original case-control study followed by systematic review and meta-analysis of existing evidence. Clin Endocrinol (Oxf). 2010;72(3):383–92.
19. Yazawa T, Inaoka Y, Okada R, et al. PPAR-gamma coactivator-1alpha regulates progesterone production in ovarian granulosa cells with SF-1 and LRH-1. Mol Endocrinol. 2010;24(3):485–96.
20. Zhu Q, Zuo R, He Y, et al. Local regeneration of cortisol by 11beta-HSD1 contributes to insulin resistance of the granulosa cells in PCOS. J Clin Endocrinol Metab. 2016;101(5):2168–77.
21. He T, Sun Y, Zhang Y, et al. MicroRNA-200b and microRNA-200c are up-regulated in PCOS granulosa cell and inhibit KGN cell proliferation via targeting PTEN. Reprod Biol Endocrinol. 2019;17(1):68.
22. Liu H, Xie J, Fan L, et al. Cryptotanshinone protects against PCOS-induced damage of ovarian tissue via regulating oxidative stress, mitochondrial membrane potential, inflammation, and apoptosis via regulating ferroptosis. Oxid Med Cell Longev. 2022;2022:8011850.
23. Song J, Luo S, Li SW. miRNA-592 is downregulated and may target LHCGR in polycystic ovary syndrome patients. Reprod Biol. 2015;15(4):229–37.
24. Livak KJ, Schmittgen TD. Analysis of relative gene expression data using real-time quantitative PCR and the 2(-Delta Delta C(T)) Method. Methods. 2001;25(4):402–8.
25. Dorostghoal M, Mahabadi MK, Adham S. Effects of maternal caffeine consumption on ovarian follicle development in wistar rats offspring. J Reprod Infertil. 2011;12(1):15–22.
26. Geng X, Zhao J, Huang J, et al. lnc-MAP3K13-7:1 inhibits ovarian GC proliferation in PCOS via DNMT1 downregulation-mediated CDKN1A promoter hypomethylation. Mol Ther. 2021;29(3):1279–93.
27. Liu Y, Liu H, Li Z, et al. The release of peripheral immune inflammatory cytokines promote an inflammatory cascade in PCOS patients via altering the follicular microenvironment. Front Immunol. 2021;12:685724.
28. Dai D, Tan Y, Guo L, Tang A, Zhao Y. Identification of exosomal miRNA biomarkers for diagnosis of papillary thyroid cancer by small RNA sequencing. Eur J Endocrinol. 2020;182(1):111–21.
29. Wu H, Yin J, Ai Z, Li G, Li Y, Chen L. Overexpression of miR-4433 by suberoylanilide hydroxamic acid suppresses growth of CML cells and induces apoptosis through targeting Bcr-Abl. J Cancer. 2019;10(23):5671–80.
30. Gong Y, Luo S, Fan P, Zhu H, Li Y, Huang W. Growth hormone activates PI3K/Akt signaling and inhibits ROS accumulation and apoptosis in granulosa cells of patients with polycystic ovary syndrome. Reprod Biol Endocrinol. 2020;18(1):121.
31. Liu Y, Zhai J, Chen J, Wang X, Wen T. PGC-1alpha protects against oxidized low-density lipoprotein and luteinizing hormone-induced granulosa cells injury through ROS-p38 pathway. Hum Cell. 2019;32(3):285–96.
32. Xu P, Gildea JJ, Zhang C, et al. Stomach gastrin is regulated by sodium via PPAR-alpha and dopamine D1 receptor. J Mol Endocrinol. 2020;64(2):53–65.
33. Komar CM. Peroxisome proliferator-activated receptors (PPARs) and ovarian function–implications for regulating steroidogenesis, differentiation, and tissue remodeling. Reprod Biol Endocrinol. 2005;3:41.
34 Sato N, Uchida K, Nakajima M, Watanabe A, Kohira T. Collaborative work on evaluation of ovarian toxicity. 13) Two- or four-week repeated dose studies and fertility study of PPAR alpha/gamma dual agonist in female rats. J Toxicol Sci. 2009;34(Suppl 1):137–46.
35. Wang DR, Wang B, Yang M, et al. Suppression of miR-30a-3p attenuates hepatic steatosis in non-alcoholic fatty liver disease. Biochem Genet. 2020;58(5):691–704.
36. Brennan KM, Kroener LL, Chazenbalk GD, Dumesic DA. Polycystic ovary syndrome: impact of lipotoxicity on metabolic and reproductive health. Obstet Gynecol Surv. 2019;74(4):223–31.
37. Lovekamp-Swan T, Jetten AM, Davis BJ. Dual activation of PPARalpha and PPARgamma by mono-(2-ethylhexyl) phthalate in rat ovarian granulosa cells. Mol Cell Endocrinol. 2003;201(1–2):133–41.
38. Froment P, Gizard F, Defever D, Staels B, Dupont J, Monget P. Peroxisome proliferator-activated receptors in reproductive tissues: from gametogenesis to parturition. J Endocrinol. 2006;189(2):199–209.
39. Fuhler GM. The immune system and microbiome in pregnancy. Best Pract Res Clin Gastroenterol. 2020;44–45:101671.
40. Zhang X, Zhivaki D, Lo-Man R. Unique aspects of the perinatal immune system. Nat Rev Immunol. 2017;17(8):495–507.
41. Pires MA, Payan-Carreira R. Resident macrophages and lymphocytes in the canine endometrium. Reprod Domest Anim. 2015;50(5):740–9.
42. Cornish EF, Filipovic I, Asenius F, Williams DJ, McDonnell T. Innate immune responses to acute viral infection during pregnancy. Front Immunol. 2020;11:572567.
43. Gordon SM, Nishiguchi MA, Chase JM, Mani S, Mainigi MA, Behrens EM. IFNs drive development of novel IL-15-responsive macrophages. J Immunol. 2020;205(4):1113–24.
44. Zheng S, et al. Mechanism of quercetin on the improvement of ovulation disorder and regulation of ovarian CNP/NPR2 in PCOS model rats. J Formos Med Assoc. 2022;121(6):1081–92.
45. Krysiak R, Kowalcze K, Okopien B. Hypothalamic-pituitary-gonadal axis and sexual functioning in metformin-treated men after discontinuation of testosterone replacement therapy: a pilot study. J Clin Pharm Ther. 2021;46(6):1764–75.
46. Peng T, Phasouk K, Bossard E, et al. Distinct populations of antigen-specific tissue-resident CD8+ T cells in human cervix mucosa. JCI Insight. 2021; 6(15).
47. Kang S, Wu Q, Huang J, et al. Tissue resident memory gammadeltaT cells in murine uterus expressed high levels of IL-17 promoting the invasion of trophocytes. Front Immunol. 2020;11:588227.
48. Weigel K, Lobsien E, Lobsien D, Brodhun M, Conrad E, Steinbrecher A. Double vision and a wrong track. Fortschr Neurol Psychiatr. 2020;88(5):331–6.

49. Makker PG, Duffy SS, Lees JG, et al. Characterisation of immune and neuroinflammatory changes associated with chemotherapy-induced peripheral neuropathy. PLoS One. 2017;12(1):e0170814.
50. O'Dwyer KM, Advani AS. When to treat adults like children: optimizing therapy for lymphoblastic lymphoma in young adults. J Clin Oncol. 2016;34(6):533–8.
51. Matsuzaki J, Tsuji T, Chodon T, Ryan C, Koya RC, Odunsi K. A rare population of tumor antigen-specific CD4(+)CD8(+) double-positive alphabeta T lymphocytes uniquely provide CD8-independent TCR genes for engineering therapeutic T cells. J Immunother Cancer. 2019;7(1):7.
52. Huang X, Liu L, Xu C, et al. Tissue-resident CD8(+) T memory cells with unique properties are present in human decidua during early pregnancy. Am J Reprod Immunol. 2020;84(1):e13254.
53. Li Z, Peng A, Feng Y, et al. Detection of T lymphocyte subsets and related functional molecules in follicular fluid of patients with polycystic ovary syndrome. Sci Rep. 2019;9(1):6040.